PNAS RESEARCH ARTICLE | EARTH, ATMOSPHERIC, AND PLANETARY SCIENCES

Zircon geochemistry from early evolved terranes records coeval stagnant- and mobile-lid tectonic regimes

Emily E. Mixon[a,1], Ann M. Bauer[a], Tyler B. Blum[a], John W. Valley[a], Hanika Rizo[b], Jonathan O'Neil[c], and Kouki Kitajima[a]

Affiliations are included on p. 7.

Edited by T. Harrison, University of California, Los Angeles, CA; received March 14, 2024; accepted August 8, 2024

Determining the mechanisms by which the earliest continental crust was generated and reworked is important for constraining the evolution of Earth's geodynamic, surface, and atmospheric conditions. However, the details of early plate tectonic settings often remain obscured by the intervening ~4 Ga of crustal recycling. Covariations of U, Nb, Sc, and Yb in zircon have been shown to faithfully reflect Phanerozoic whole-rock-based plate-tectonic discriminators and are therefore useful in distinguishing zircons crystallized in ridge, plume, and arc-like environments, both in the present and in deep time. However, application of these proxies to deciphering tectonic settings on the early Earth has thus far been limited to select portions of the detrital zircon record. Here, we present in situ trace-element and oxygen isotope compositions for magmatic zircons from crystalline crustal rocks of the Acasta Gneiss Complex and the Saglek-Hebron Complex, Canada. Integrated with information from whole-rock geochemistry and zircon U-Pb, Hf, and O isotopes, our zircon U-Nb-Sc-Yb results reveal that melting of hydrated basalt was not restricted to a single tectonomagmatic process during the Archean but was operative during the reworking of Hadean protocrust and the generation of juvenile crust within two cratons, as early as 3.9 Ga. We observe zircon trace-element compositions indicative of hydrous melting in settings that otherwise host seemingly differing whole-rock geochemistry, zircon Hf, and zircon O isotopes, suggesting contemporaneous operation of stagnant-lid (oceanic plateau) and mobile-lid (arc-like) regimes in the early Archean.

Archean | zircon | crustal evolution | isotope geochemistry

Significance

Much of our knowledge of early Archean crustal processes comes from the detrital zircon record, in which zircons are separated from their parental lithologic context. Our observation of paired zircon trace elements and oxygen isotope compositions from crystalline crustal rocks hosted in two of the most ancient crustal fragments (Acasta and Saglek) therefore affords a unique opportunity to 1) assess suites of magmatic zircon crystallized within the same host rock and 2) leverage correlations between zircon and whole-rock geochemistry. Acasta and Saglek have shared zircon U-Nb-Sc-Yb tectonic proxy values, indicative of hydrous melting, but differ in other geochemical systems, suggesting that hydrous melt processes took place in a diversity of coeval tectonic regimes on the early Earth.

The detrital zircon record indicates that relatively cool, hydrous surface conditions existed in the Hadean and that materials formed and altered at low temperatures were incorporated into felsic crustal magmas prior to 4.03 Ga (1–3). However, the details of early plate tectonic settings remain obscured by the intervening 4 Ga of dynamic crustal recycling, and debate remains concerning the style of plate tectonics responsible for reworking the earliest crust throughout the Archean (4–6). Given the comparative geochemical retentiveness of zircon relative to rocks, zircon is often used as a robust archive of the earliest crust formation. Therefore, quantifying and interpreting the processes controlling correlations between zircon and whole-rock geochemistry across a range of Phanerozoic tectonic settings (7, 8) may serve as a powerful framework for making inferences about tectonic provenance across geologic time, particularly when the zircon record might represent the only, or most reliable, geochemical archive—such as in the early Archean. Specifically, covariation of trace elements (TE) U, Nb, Sc, and Yb in zircon has been shown to distinguish among mid-ocean-ridge-type (MOR) zircon, ocean-island-type (OI) zircon, and arc-type zircon in modern plate-tectonic regimes (8). In contrast to their behavior in magmatic systems, U and Yb exhibit comparable affinity in zircon. As a result of this compatibility and the large abundance range of U in zircon, ratios of U, Yb, and other HREE in zircon can be interpreted to reflect the composition of the melt at the time of zircon crystallization (8). Notably, depletion of Nb relative to U can distinguish between zircons from MOR or OI melts (generally falling below U/Nb of 20) and those generated by arc-like (or more broadly for our purposes in the Archean, "hydrous") processes. Scandium enrichment relative to Yb in zircon (Sc/Yb mantle array = 0.1) is also a useful proxy for identifying the melting of hydrated material, as Sc can track the fractionation of ferromagnesian minerals (amphibole and/or clinopyroxene). While in the Phanerozoic, hydrous flux melting is canonically associated with subduction zone magmatism (9), decades of study show that the Archean whole-rock record is dominated by lithologies (e.g., tonalite–trondhjemite–granodiorite, sanukitoids, komatiites) which differ significantly from those observed in modern arc rocks (5, 10–13). Thus, flux melting conditions in the Archean likely occurred in tectonic regimes different than those operative today, due to evolving mantle conditions (14, 15). Proposed geodynamic environments for this period, in which tonalite-trondhjemite-granodiorites (TTGs)

Author contributions: E.E.M., A.M.B., and T.B.B. designed research; A.M.B., H.R., and J.O. contributed samples; T.B.B. and K.K. contributed new reagents/analytic tools; E.E.M., T.B.B., and K.K. analyzed data; E.E.M. drafted the initial manuscript; and E.E.M., A.M.B., T.B.B., J.W.V., H.R., J.O., and K.K. wrote the paper.

The authors declare no competing interest.

This article is a PNAS Direct Submission.

[1]To whom correspondence may be addressed. Email: eemixon@wisc.edu.

This article contains supporting information online at https://www.pnas.org/lookup/suppl/doi:10.1073/pnas.2405378121/-/DCSupplemental.

Published September 16, 2024.

were generated by melting of hydrated basalt, include episodic and/or "squishy" subduction (16, 17), heat-pipe volcanism (18), delamination melting (19, 20), and convective overturn or drips within oceanic plateaus (21, 22). Despite this diversity of proposed regimes, it has been demonstrated that continental crust at ~4 Ga had U/Yb, Nb/Yb, and Nb/Sc ratios within a factor of two of Phanerozoic values, broadly maintaining their utility for identifying "hydrous" melt generation, regardless of tectonic setting (23).

Due to the paucity of preserved Archean rocks, and the challenges associated with analysis of Sc and Nb in zircon (*SI Appendix*, Supporting Information), application of proxies involving Sc or Nb to the earliest crust has so far been limited to select populations of detrital zircons (23–25). Additionally, even in the Phanerozoic, interpretation of single or ambiguously grouped detrital zircon TE analyses (e.g., zircons which are binned together by U-Pb age but are likely to reflect multiple sources) is more likely to result in erroneous provenance associations (8). Therefore, given the possible diversity of settings in which hydrous melting might have occurred in the early Earth, it is advantageous to compare zircon TE discriminators from cogenetic suites of zircon hosted within crystalline crustal rocks, as opposed to clastic rocks containing detrital zircons potentially formed from diverse settings. Working with igneous zircon from preserved exposed terranes, rather than detrital zircons for which magmatic sources may be variable or unknown, allows additional correlation of zircon TE information with zircon isotopic and whole-rock geochemical context. This integrated approach allows improved description of the characteristics of tectonic regime(s) where hydrous melting was operative during the production of the earliest continental crust.

Here, we present paired zircon $\delta^{18}O$ and TE compositions for suites of zircon from eight granitoid rocks of the Acasta Gneiss Complex (AGC) in the NW Territories, Canada, and seven granitoids from the Archean crust of the Saglek-Hebron Complex (SHC) in Labrador, Canada. All 15 orthogneisses studied span ~3.9 to ~2.8 Ga in crystallization age (Fig. 1). The AGC and SHC are compositionally diverse polymetamorphic terranes that preserve some of the oldest known zircon-bearing crustal rocks (26–31). The AGC whole-rock TE and zircon Lu-Hf isotopic record has been interpreted as recording a transition from melting of Hadean protocrust in a stagnant-lid tectonic regime to

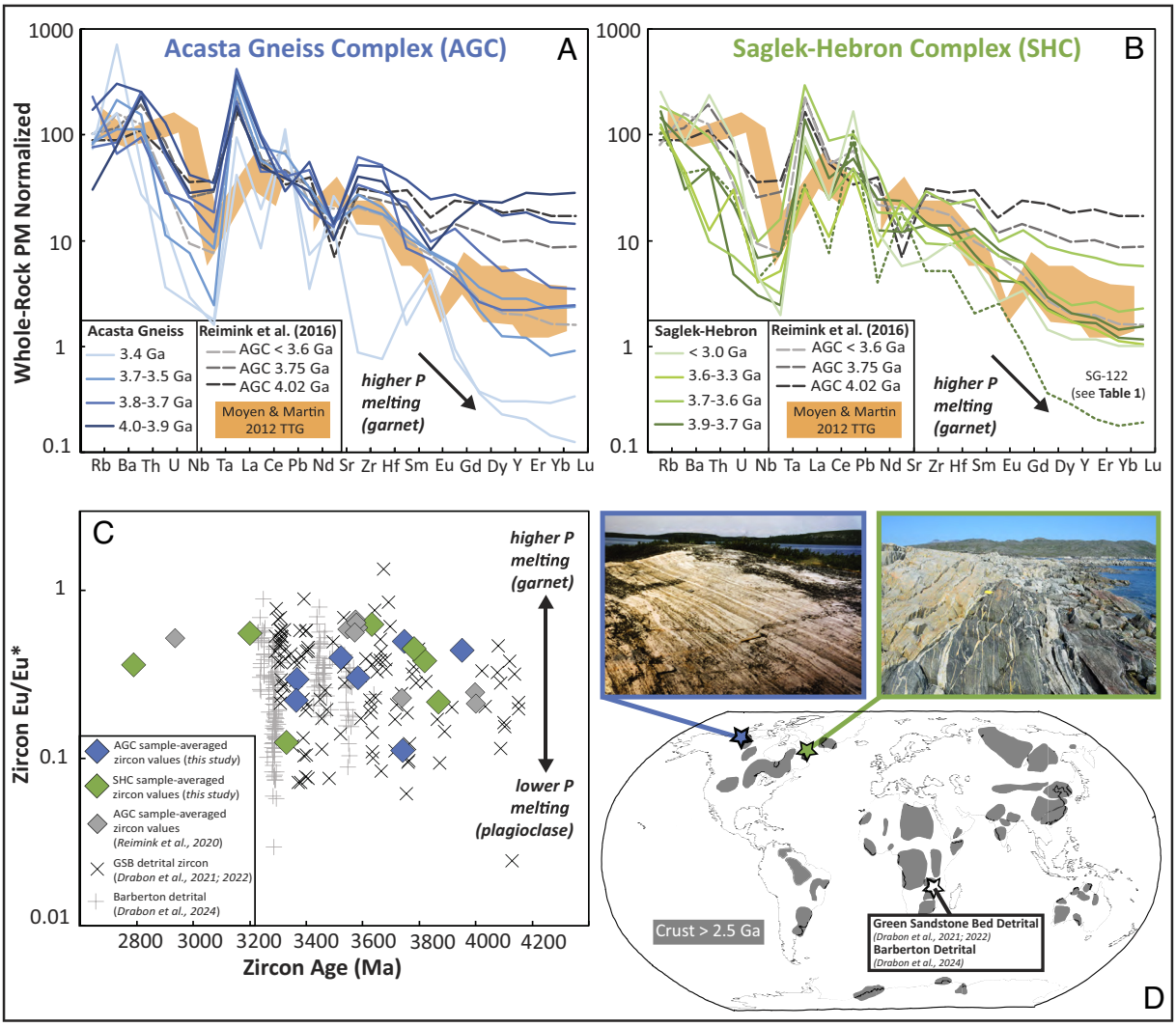

Fig. 1. (*A* and *B*) Primitive-mantle normalized (35) whole-rock TE plots for AGC (blue) and SHC (green) gneisses, showing heavy REE depletion relationships with age. Published AGC whole-rock data (32) and average Archean TTGs (5) are shown for comparison. AGC and SHC whole-rock data for samples from this study are found in Dataset S1. (*C*) Sample-averaged (all zircon analyses that pass screening criteria within a rock) Eu/Eu* for AGC and SHC (*Materials and Methods*, this study) with higher zircon Eu/Eu* values denoting higher pressure melting. Detrital zircon analyses from Green Sandstone Bed (GSB) and broader Barberton studies (23–25) shown for comparison. Note that screening criteria for this study and previously published data differ. Zircon Eu/Eu* uncertainties are smaller than symbol size. (*D*) Map displays locations of the AGC (photo from Sam Bowring), SHC, and GSB relative to global Archean crust distribution.

inception of mobile-lid tectonics at 3.6 Ga (32, 33); the similar temporal progression of zircon Hf isotope systematics in other terranes has been proposed to record this shift in tectonic styles globally at ~3.8 to 3.6 Ga (34). To interrogate this model, we apply a workflow (*SI Appendix*, Fig. S13) prioritizing characterization of zircon alteration and spatial correlation of multiple geochemical systems within primary grain domains. Leveraging context from zircon U-Pb and Hf isotopes and whole-rock geochemistry for the AGC and SHC, we present paired zircon oxygen isotope and U-Nb-Sc-Yb focused zircon TE compositions for Archean orthogneisses from two of Earth's oldest known crustal fragments.

Results

We performed 323 oxygen isotope analyses on 197 AGC zircons with previously assigned crystallization ages from 3.95 to 3.36 Ga. Of these, 201 analyses pass screening criteria (Datasets S2 and S3 and *Materials and Methods*) and give zircon $\delta^{18}O$ values that range from +5.2 ‰ to +7.0 ‰ (Dataset S4). Zircon $\delta^{18}O$ results for 108 zircons from seven SHC orthogneisses with crystallization ages spanning 3.87 to 2.79 Ga are reported in ref. 36. Of the 271 SHC zircon oxygen isotope analyses, 208 meet screening criteria (*Materials and Methods*) and have zircon $\delta^{18}O$ values ranging from +5.0 ‰ to +8.4 ‰. Fig. 2*B* shows $\delta^{18}O$ isotope analyses from AGC and SHC that pass screening and are considered to represent primary geochemistry.

Following zircon $\delta^{18}O$ analysis, we performed SIMS TE analyses on 145 AGC zircon domains (n =125 grains) and 135 SHC zircon domains (n = 108 grains) identified as preserving primary zircon $\delta^{18}O$. All TE data can be found in Datasets S5 and S6. For analyses that pass screening (n = 100 AGC, n = 82 SHC), we observe chondrite-normalized rare earth element (REE) patterns with light REE depletion and heavy REE enrichment (*SI Appendix*, Fig. S4), further indicative of primary geochemistry (38–40). Rock-averaged zircon analyses (average of all analyses that pass screening criteria for a given sample) have U/Nb between 26 and 76 for the SHC, and 29 and 195 for the AGC, respectively (*SI Appendix*, Table S1). Rock-averaged zircon Sc/Yb ranges are 0.15 to 2.65 for the SHC, and 0.17 to 0.53 for the AGC (*SI Appendix*, Table S1). Trace-element ratios displayed in Figs. 2–4 are drawn from AGC and SHC TE analyses that pass screening criteria (Datasets S2 and S3 and *Materials and Methods*).

We performed 227 U-Pb analyses on AGC zircon identified as recording primary $\delta^{18}O$ and/or primary TE compositions to further screen for primary geochemistry. Of these, 198 of 227 are between 95% and 105% concordant (*SI Appendix*, Table S8). Oxygen isotope and TE analyses in SHC zircons were targeted in domains with interpreted primary U-Pb crystallization ages (31). For the purposes of discussion, AGC and SHC zircon $\delta^{18}O$ and TE data that pass screening criteria are plotted at the crystallization ages of their host rocks (refs. 27, 41; Fig. 2).

Discussion

Petrogenetic Insights from Integrated Whole-Rock and Zircon Geochemistry. While geochemistry of zircon can serve as a monitor of parental melt composition, estimates of zircon-melt partition coefficients often vary by an order of magnitude and are strongly influenced by temperature, especially when considering the REE, which behave consistently with lattice strain models (8, 43–45). Although additional complexities may emerge when considering crustal rocks generated by multiple melting events, change in U/Yb due to melt fractionation is small compared to initial differences between MOR, OI, and arc sources (8). Thus, direct observation of multiple TE ratios (e.g., Nb/Yb, U/Yb, Sc/Yb) applied in tandem (Figs. 2 and 3 and *SI Appendix*, Figs. S6–S8) minimizes compositional variation due to temperature when comparing different zircon populations from distinct tectonic settings, improving the identification of melt regimes over studies reliant on absolute TE concentrations or partition coefficient models. Furthermore, although whole-rock chemistry may in some cases be disturbed, correlating multiple geochemical systems across the mineral and rock scales can aid in making robust interpretations about primary Archean geochemistry. In this context, our application of multiple zircon TE discriminators to crystalline crustal rocks preserved in the AGC and SHC affords a unique opportunity to assess cogenetic suites of zircon by investigating zircon isotopic information, zircon TEs, and whole-rock geochemistry from the same rocks (Fig. 2 and *SI Appendix*, Figs. S8–S11). At Acasta, there is a steepening of whole-rock REE patterns through time (23), which is reproduced in our AGC samples (Fig. 1*A* and Dataset S1). Titanium isotope compositions of orthogneisses in the AGC record a similar temporal evolution in melt regime, with a transition from exclusively intraplate tholeiitic compositions to the appearance of hydrated calc-alkaline-like magmatism at 3.8 Ga (46), contemporaneous with whole-rock, quartz, and zircon Si-O isotope evidence for the Eoarchean appearance of surface silicon recycling (47). In comparison, felsic gneisses from Saglek do not display a systematic relationship between age and whole-rock chemistry, with evidence of deep-seated melting in the presence of residual garnet apparent as early as 3.9 Ga, followed by REE patterns reflective of variable melting depths thereafter (ref. 31; Fig. 1*B* and Dataset S1).However, primary zircon chemistry in both the AGC and SHC consistently records elevated U-Nb-Sc-Yb proxies (U/Nb > 20 and Sc/Yb > 0.1) from 3.9 Ga onward, consistent with Eoarchean melt compositions resulting from the melting of hydrated parental material (*SI Appendix*, Table S1 and Figs. 2–4). When integrated with the whole-rock context (Fig. 1*C*), our zircon TE records for the AGC and SHC agree with Hadean and Archean zircon-melt models that generate REE patterns suggestive of hydrous melt generation in the presence of garnet and/or amphibole (48, 49).

Although multiple zircon TE provenance proxies suggest that hydrous melting was operative in the SHC and AGC in the Eoarchean, differences in whole-rock REE (Fig. 1) and dissimilar zircon ε_{Hf}, and $\delta^{18}O$ records between the localities (Fig. 2 *A* and *B*) point to differences in the magmatic sources and potential tectonic regimes responsible for this hydrous melt signature. While zircon initial ε_{Hf} from the AGC indicates a shift toward more juvenile compositions at ~3.6 Ga (41), zircon Hf systematics from the SHC suggest early juvenile crustal growth at ~3.87 Ga alongside remelting of a Hadean protocrust throughout the Paleoarchean, followed by a brief and highly localized juvenile source ~3.22 Ga, and a suite of Neoarchean granites interpreted to have formed via reworking of Eoarchean TTGs (31, 50). Furthermore, the zircon $\delta^{18}O$ record includes rocks of uniquely high (≥ 6.5‰) $\delta^{18}O$ ca. 3.6 and 3.3 Ga in the SHC (36), whereas zircon $\delta^{18}O$ remains uniform and mildly elevated in the AGC (Fig. 2*B*). These differing zircon $\delta^{18}O$ systematics from the two cratons (Fig. 2 and *SI Appendix*, Table S1 and Fig. S11) indicate that incorporation of sediments can be highly variable and localized in Archean hydrous melts and suggests that felsic crustal genesis was largely driven by the recycling of hydrated oceanic crust and other mafic material, rather than voluminous contributions from sediments or other

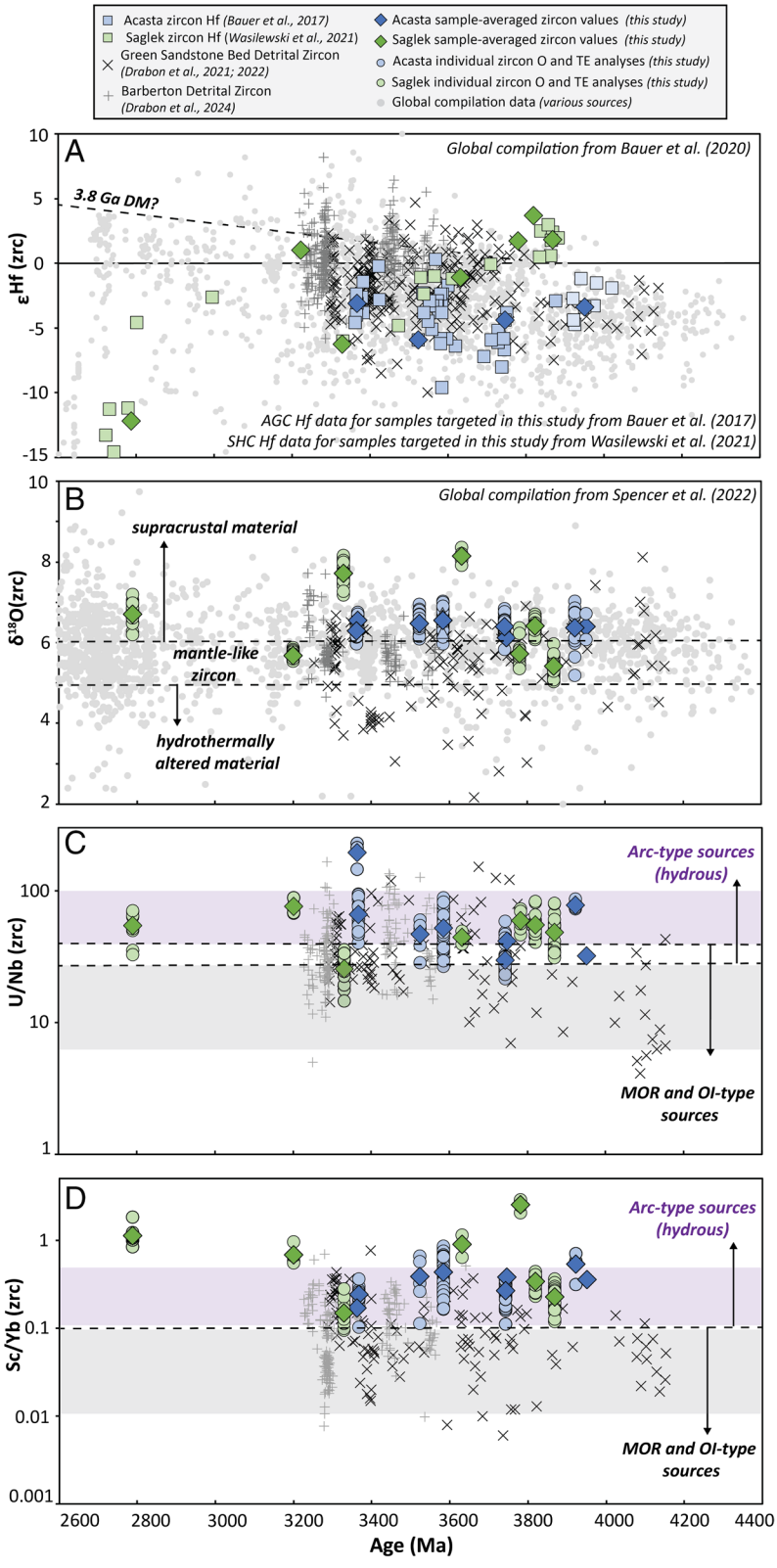

Fig. 2. Time series of zircon isotope and TE data. (*A*) Compiled global zircon ε_{Hf} data (34). Samples targeted by the current study are shown as diamonds. Juvenile compositions are interpreted as those closest to DM. (*B*) Zircon $\delta^{18}O$, with global compilation from ref. 37. (*C*) Zircon U/Nb. (*D*) Zircon Sc/Yb. Diamonds in Panels *B*, *C*, and *D* represent rock-averaged zircon data (all analyses that pass screening criteria from a given rock) for AGC and SHC gneisses, while colored circles show data range of individual zircon analyses (*Materials and Methods*). Colored bars (*C* and *D*) depict the first to third quartile of typical Phanerozoic arc-like and MORB/OIB sources (8). *X*'s in all panels denote detrital GSB data from ref. 24, and crosses denote detrital Barberton zircon from ref. 25.

high- $\delta^{18}O$ parental material. This is consistent with other observations of the prevalence of only mildly elevated zircon $\delta^{18}O$ values before 2.5 Ga (51) and with observations that the zircon $\delta^{18}O$ of S-type granites in the Superior, Slave, and North China cratons increases from 6.2 ± 1.3‰ to 9.9 ± 2.2‰ (2σ) across the Archean–Proterozoic boundary (52).

In the context of Hf and $\delta^{18}O$, our zircon U-Nb-Sc-Yb results demonstrate that despite variations in 1) melt depth as inferred from AGC and SHC whole-rock chemistry (Fig. 1), 2) melt source as tracked by zircon Hf isotopes (Fig. 2*A*), and 3) sedimentary influence as inferred from non-mantle-like high-$\delta^{18}O$ sources (Fig. 2*B*); melting of hydrated basalt was the primary mechanism for the genesis of zircon-bearing magmas in both the AGC and SHC as early as 3.9 Ga (Figs. 2–4). The persistence of U-Nb-Sc-Yb ratios consistent with hydrous melting across multiple magmatic generations of differing source character in the AGC and SHC further suggests

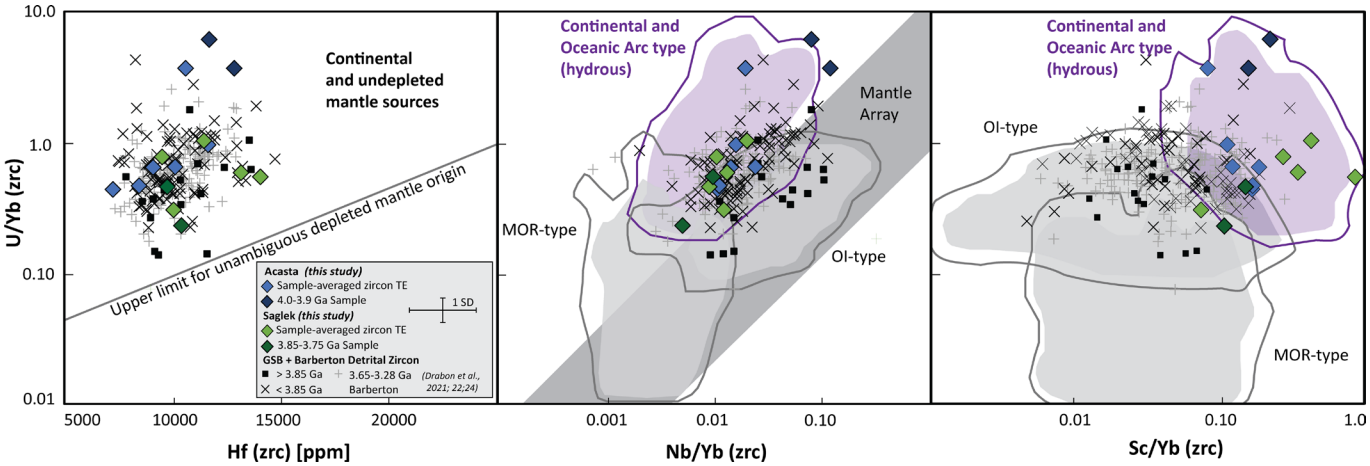

Fig. 3. Zircon TE bivariate plots after Grimes et al. (8). All AGC and SHC data presented pass screening criteria (*Materials and Methods*). AGC (blue) and SHC (green) data are displayed as rock-averaged zircon values for individual samples (ages shown in Fig. 2). Eoarchean samples are darker blue and darker green, respectively. Detrital GSB data (X and squares) from ref. 24 and Barberton (+) from ref. 25 shown for comparison, with squares representing zircons > 3.85 Ga. Colored fields and contour lines (95% level) represent tectonic affinities defined by the compilation from ref. 8.

that hydrous petrogenesis of felsic rocks was not restricted to a single magmatic source type in the early Archean. Instead, hydrous petrogenesis was likely operative during both the early reworking of Hadean protocrust and the later generation of juvenile material.

Evidence for Eoarchean Hydrous Melting in Vertical and Horizontal Tectonic Regimes. Zircon U-Nb-Sc-Yb systematics from the AGC and SHC indicate that in two distinct terranes, hydrous melting processes preceded the proposed mid-to-late Archean global shift(s) in tectonic regime and crustal volume, based on zircon Hf and $\delta^{18}O$ (34, 53–55). A variety of geodynamic scenarios have been proposed to reconcile geochemical observations, ranging from stagnant (oceanic plateau or plume, orogenic collapse/'sagduction') to mobile (hot or shallow "subduction", convective overturn) regimes (3, 6). The low-pressure TTG whole-rock HREE profiles (Fig. 1*A*) and relatively low zircon Eu/Eu* (Fig. 1*C*) at 3.9 Ga in the AGC coincide with amphibole-present melting (Sc-enriched zircon) (Fig. 2*D*, Fig. 4)—a pattern which could be generated in a plateau or "sagduction" profile, where hydrated rocks are confined to the upper 10 s of kilometers and heat flow is driven by intraplate intrusive magmatism (16, 56). While a full complement of zircon U-Sc-Nb-Yb data does not exist for the oldest (4.02 Ga) Idiwhaa unit of the AGC, zircon U-Yb, zircon $\delta^{18}O$, and whole-rock chemistry, including Ti and Si isotopes, are consistent with intraplate tholeiitic magmatism >3.9 Ga (32, 33, 46–48).

However, the coupling of higher-pressure TTG whole-rock HREE profiles (Fig. 1) with the onset of juvenile zircon ε_{Hf} and zircon U-Nb-Sc-Yb signatures consistent with hydrous melting (Fig. 2) in the SHC at 3.9 Ga and AGC at 3.6 Ga suggest significant

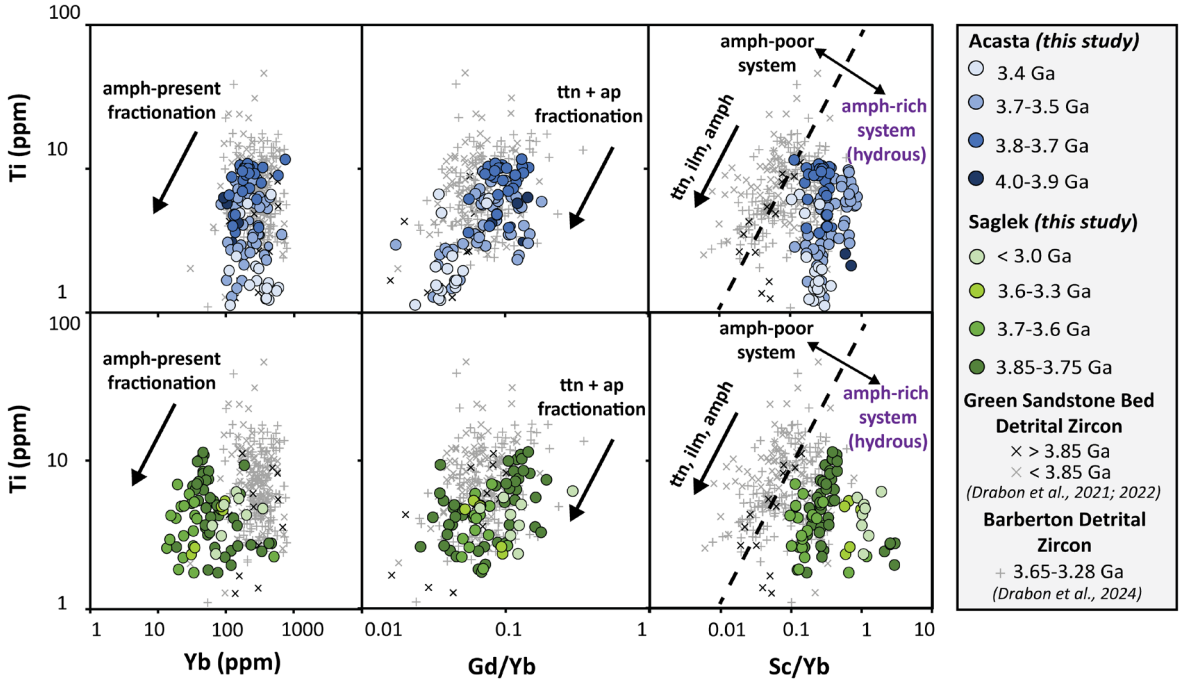

Fig. 4. Petrogenetic diagrams of individual zircon analyses from the AGC (blue) and SHC (green) and detrital GSB (X and squares) and Barberton zircon (+), showing influence of amphibole fractionation in later-formed zircon (trends from ref. 8). Magmatic generations are defined by (refs. 41, 42 AGC) and (ref. 31, SHC) and are shown in *SI Appendix*, Table S1. Relatively elevated Sc/Yb of AGC and SHC zircon is inferred to result from zircon growth in equilibrium with amphibole-saturated melt, while decreasing Sc/Yb and Gd/Yb with increasing Ti for all three zircon localities (AGC, SHC, GSB/Barberton) likely reflects open-system fractional crystallization.

hydrous melt formed at increased pressures (corresponding with modern geochemical signatures indicative of garnet stability, onset ~35 to 50 km in mafic rocks). While recent work has highlighted that whole-rock granitoid and zircon crustal thickness proxies may be limited in their applicability to the early Earth (57), modeling suggests that "high-pressure" (~50 to 70 km) TTG chemistry may still represent decreasing residual plagioclase under a hotter geotherm at more moderate crustal depths (~30 to 40 km) due to increasing water content from hydrous melting (58). Despite the uncertainties in applying modern crustal thickness proxies to the Precambrian, melts generated at greater pressure should exhibit higher zircon Eu/Eu* (Fig. 1*C*) and whole-rock and zircon Dy/Yb (*SI Appendix*, Fig. S10) (59, 60). Therefore, geochemical proxies consistent with relative increases in pressure (even if produced at moderate rather than extreme crustal depths), together with the requirement from U-Nb-Sc-Yb ratios for hydrous melting as early as 3.9 Ga in the SHC, limits the likelihood of a solely vertical or stagnant-lid tectonic regime in the Eoarchean. This conclusion aligns with thermal modeling constraints, which suggest it is anomalous or unlikely to have water and basaltic melts coexisting at the lower crustal depths necessary to generate voluminous felsic melts with coupled high-pressure and hydrated signatures (~40 km, refs. 5, 61).

Zircon and whole-rock indicators of hydrous melting and relative pressure provide constraints which permit models wherein thick oceanic crust, shallow subduction angles, and higher mantle temperatures could yield an episodic subduction regime (15, 16, 62). Regional and global mantle convection models produce a cycle of slab sinking, thinning, and detachment with relatively short timescales at high mantle temperatures (e.g., ~5 to 10 Myr at 1750 to 1900 K), (16). Short-lived subduction cycles could also reconcile nearly contemporaneous tholeiitic Eoarchean mafic rocks in the SHC (31, 63) with our interpretation of a subduction origin for the oldest SHC felsic crust. Given the low geochronologic resolution of ancient mafic rocks, SHC metavolcanic units which lack subduction signatures could have occurred during a ~5 to 10 Myr slab detachment sequence, where upwelling mantle contributions dominate during nonsubduction episodes—a process that has been proposed for other Archean terranes with alternating "arc" and "nonarc" igneous compositions (64). The global coexistence of multiple tectonomagmatic regimes, including possibly short-lived subduction cycles, is consistent with multiple lines of geochemical evidence including 1) variable contribution from juvenile Hf reservoirs (Fig. 2*A*) in the SHC (3.9 Ga, 3.2 Ga) and the AGC (< 3.6 Ga), 2) differing zircon δ^{18}Ovalues for the two terranes (Fig. 2*B*), and 3) μ^{142}Nd signatures which record long-lived reworking of older crustal material from 3.9 to 3.3 Ga in the SHC (*SI Appendix*, Table S1), (50) and from 4.0 to 3.8 Ga in the AGC (33).

Comparison of Acasta and Saglek TE Geochemistry with Detrital Hadean-Archean Zircons. Our TE tectonic provenance proxy values for AGC and SHC igneous zircons ca. 3.9 Ga can be compared with published U-Nb-Sc-Yb data from detrital zircons from the Hadean-Archean Green Sandstone Bed (GSB) from the Barberton Greenstone Belt (Figs. 1 *C* and *D* and 2 *C* and *D*) (Kaapvaal Craton, South Africa), (23–25). Unlike 3.9 to 3.0 Ga AGC and SHC zircons, which consistently fall in the Phanerozoic continental or oceanic arc-like fields defined by (8), GSB detrital zircons >3.8 Ga record OIB-like U-Nb-Sc-Yb signatures (e.g., U/Nb < 20 and Sc/Yb < 0.1) before 3.8 Ga, followed by a roughly equal distribution between hydrous (arc-like) and OIB-like mantle sources thereafter (U/Nb of 7 to 151, Figs. 2 and 3), (23, 24). Comparing the detrital and igneous records is complicated, given that we observe a broad range of zircon U-Nb-Sc-Yb ratios within a single granitoid (*SI Appendix*, Table S1 and Fig. 2 *C* and *D*), meaning that interpreting data scatter in a detrital record is obscured by the primary geologic variability of the individual source rocks. The presence of a wider range toward higher zircon Ti concentrations (8 to 16 ppm) correlated with lowest U/Nb and Sc/Yb in GSB and Barberton detrital zircons (*SI Appendix*, Fig. S6), (23–25) is consistent with a mix of source lithologies in the detrital record, while even the oldest AGC and SHC zircons record Ti concentrations more typical of Phanerozoic felsic rocks (65). The more equant distribution of mantle sources in Archean detrital zircons from the GSB, paired with the absence of OIB-like U/Nb and Sc/Yb values in rock-averaged zircon values for the SHC and AGC granitoids 3.9 to 2.8 Ga (Fig. 2 and *SI Appendix*, Table S1), could suggest geochemical decoupling of zircons from crystalline igneous rocks (putative plutonic sources) and detrital zircons (putative shallow volcanic sources), as has been posited for the zircon δ^{18}O record (37). Alternatively, the higher variability of zircon U/Nb and Sc/Yb in the Archean GSB when compared to the AGC and SHC could more simply reflect a mixture of multiple parental rocks/terranes, when compared to the smaller range of values recorded in any single cogenetic suite of zircons sourced from 15 known parent rocks (our AGC and SHC data). Regardless, zircon TE tectonic proxies from all localities—AGC, SHC, and GSB—reflect little to no evidence for the significant petrogenetic role of a nominally dry MOR-depleted mantle source of felsic crust formation in the early Archean (Fig. 3). Combined, the zircon U-Nb-Sc-Yb systematics from these three terranes further imply that the zircon record reflects a diversity of Eoarchean tectonomagmatic domains coexisting on a global scale.

Implications. U/Yb, Nb/Yb, and Nb/Sc ratios in the AGC and SHC reflect early (ca. 3.9 Ga) onset of hydrous melt processes during the generation of continental crust. When integrated with additional geochemical context from whole-rock geochemistry and zircon Hf and δ^{18}O, these zircon TE provenance proxies are inconsistent with lone operation of stagnant or vertical tectonics (5, 56, 61). Instead, key geochemical and isotopic differences between the AGC and SHC, and between these suites of magmatic zircons and the detrital zircon record, suggest that melting of hydrated mafic material to produce felsic crust was operative during both the reworking of Hadean protocrust and the generation of juvenile material within multiple cratons, reflective of a degree of tectonic diversity in the early Earth. These observations are consistent with the notion that the early, though perhaps diachronous or episodic, initiation of lateral tectonics could have been responsible for the creation of significant volumes of continental crust on the early Earth (17, 66, 67). Differences in the magnitude and timing of the appearance of hydrous melt signatures in the AGC and SHC in comparison to the detrital record indicate that either: 1) Eoarchean hydrous melting was the result of a diversity of tectonomagmatic processes contemporaneously operating across multiple source terranes, and/or 2) that detrital and igneous zircon TE records are possibly decoupled during the Archean. Additional high temporal resolution zircon U-Nb-Sc-Yb information for more localities is necessary to distinguish these possibilities.

Materials and Methods

Geologic Context. The AGC (Fig. 1 *A* and *C*) comprises a large exposure of basement gneisses (>1,300 km^2) along the western margin of the Slave craton, Canada. Previous zircon U-Pb and Lu-Hf isotopic data from the oldest region of the AGC define multiple magmatic generations spanning 4.02 to 2.9 Ga (26, 27, 41, 68, 69). Whole-rock REE patterns have been interpreted in tandem with zircon δ^{18}O and TE from the 4.02 Ga Idiwhaa unit and later 3.75 and 3.5 Ga TTG to record a transition from relatively shallow and dry melting of Hadean mafic crust to deeper-crustal melting of hydrated Archean mafic crust after ~3.6 Ga

(Fig. 1*A*), (32, 33, 48). Due to a protracted metamorphic history, AGC zircon populations are variably complex, often containing multiple age domains and varying degrees of radiation damage, making identification of primary geochemical compositions challenging (70). We used existing zircon U-Pb and Lu-Hf isotope data to select eight AGC gneisses that have primary igneous crystallization ages and Hf isotope systematics representative of the 4.0, 3.8, 3.6, and 3.4 Ga magmatic generations (41, 42).

The SHC (Fig. 1 *B* and *C*) is a polymetamorphic terrane within the Saglek block of the Nain Province of the North Atlantic Craton, Canada. Paired zircon U-Pb and Lu-Hf isotope characterization of the Saglek-Hebron felsic gneisses has refined the chronology for magmatic generations emplaced from 3.87 to 2.79 Ga (31) with at least two granulite-facies metamorphic events recorded at ~3.6 and ~2.7 Ga (71–73). Our zircon TE data come from seven orthogneisses which were previously analyzed for U-Pb and Lu-Hf (31) and zircon $\delta^{18}O$ (36) with igneous crystallization ages ~3.85 to ~2.78 Ga.

Zircon U-Pb, Oxygen Isotope, and Trace-Element Analysis by SIMS. In situ zircon O-isotope and TE analysis for AGC and SHC zircons was performed using the CAMECA-IMS 1280 Secondary Ion Mass Spectrometer (SIMS) at the WiscSIMS Lab, University of Wisconsin-Madison (*SI Appendix*, Supplemental Text and Dataset S4). After O isotope analysis, twenty-six major and trace elements, including Al, P, Ca, Sc, Ti, Fe, Y, Nb, REE, Ta, Th, and U were measured. During TE analysis, the mass spectrometer was operated at a nominal mass resolving power of $M/\Delta M \approx 12{,}500$, sufficient to resolve major interferences for analyzed species (*SI Appendix*, Fig. S12 and Datasets S5 and S6 and *SI Appendix*, *Supplemental Text*), (74). SIMS Zircon U-Pb isotope measurements (*SI Appendix*, *Supplemental Text* and Dataset S7) were subsequently performed on AGC grain domains characterized by SEM-CL imaging and $\delta^{18}O$ and TE analysis. Saglek zircon domains targeted for $\delta^{18}O$ and TE analyses were previously dated by LA-ICP-MS (31).

Pre- and Postanalysis Screening for Altered Zircon. In SHC zircons, $\delta^{18}O$ (36) and TE analyses (this study) were targeted in the same grain domains where previous U-Pb and Lu-Hf analyses had been performed and were interpreted to represent primary crystallization ages (31). Additionally, to investigate the current damage state of SHC zircons, we performed Raman spectroscopy adjacent to SIMS analytical pits on a subset of grains representing the range of ages, CL textures, and zircon $\delta^{18}O$ in the terrane (36). AGC zircons were selected from gneisses characterized by zircon U-Pb and Lu-Hf (41). Grains were selected from nonmagnetic MEI separates. All zircons were imaged using cathodoluminescence (CL) and secondary electron (SE) techniques, and images were used to guide analytical targets (Dataset S8). After data acquisition, zircon domains targeted for oxygen-isotope and trace-element analysis were evaluated by the following tests for alteration: U-Pb age concordance, nonformula trace elements indicative of open-system behavior (Ca, Al, Fe, and La), and $^{16}OH/^{16}O$ (OH/O hereafter) and also using postanalysis imaging of the pit locations to ensure analytical spots did not intersect cracks, or result in nonideal analytical conditions (*SI Appendix*, Fig. S13).

Values of background-corrected OH/O correlate positively with these other indicators of alteration, such as elevated concentrations of nonformula elements in zircon (e.g., Al, Ca, Fe, LREEs, (38, 70, 75), radiation damage state, and recrystallization textures (76–79). Background-corrected OH/O was calculated following (77), and is corrected based on OH/O measured on a nominally anhydrous SIMS zircon running standard (UWZ1). The OH/O background varies with vacuum pressure, which changes systemically over time, as well as on a sample-to-sample and session-to-session basis (77–79). Therefore, background-corrected OH/O is not a quantitative measure of water but represents an internally consistent, relative measure of elevated water content. Background-corrected OH/O values range from -4×10^{-5} to 2×10^{-3} for the SHC and -7×10^{-5} to 1×10^{-2} for the AGC. Analyses with OH/O > 2×10^{-4} are considered unreliable (*SI Appendix*, Fig. S1). The majority (> 65%) of analyses with elevated OH/O coincide with imperfections identified during postanalysis imaging of the analytical pit, such as an inclusion or crack, suggesting that most visibly intact zircons in our study have OH/O < 2×10^{-4}. Zircon domains where $\delta^{18}O$ and TE data were obtained were screened using OH/O criteria and a 100-ppm threshold for each of Ca, Fe, and Al (*SI Appendix*, Fig. S2). These thresholds are comparable to common cutoffs of Ca and Fe >50 to 100 ppm (8, 23–25, 70). Many flagged domains based on Ca, Fe, and Al data also display high La concentration (>1 to 10 ppm) and no Ce anomaly, traits which can correlate with alteration (39, 40), *SI Appendix*, Fig. S4. Saglek zircon domains for $\delta^{18}O$ and TE analysis were preselected based on concordance of U-Pb ages and Lu-Hf isotopes interpreted by Wasilewski et al (31) to reflect primary crystallization. Acasta zircon domains for $\delta^{18}O$ (Dataset S4) and TE (Datasets S5 and S6) analysis were screened at 95 to 105% U-Pb concordance threshold, following U-Pb analyses placed in the $\delta^{18}O$ and TE domains (Dataset S7).

Despite applying a variety of preselection criteria before beginning our $\delta^{18}O$-TE analytical campaign (e.g., U-Pb ages, Lu-Hf isotopes, CL images), many of the zircons we analyzed are sufficiently complex such that our rigorous screening procedures result in a low percentage of analyses considered to preserve primary $\delta^{18}O$ and TE chemistry (*SI Appendix*, Table S1 and Fig. S13). This suggests that Archean zircons across multiple terranes/sources may have similar preservation challenges. As demonstrated in *SI Appendix*, Figs. S2, S3, and S11, our full, unfiltered dataset (with altered data denoted by open symbols) would overrepresent the trends we observe in the primary zircon chemistry. Given this trend, and the degree of variability we see in filtered/unaltered data from a given rock (e.g., Fig. 2 and *SI Appendix*, Table S1), the interpretation of highly variable detrital data, where host rocks are not known, and zircon analyses cannot be meaningfully grouped into cogenetic populations, might result in geologically meaningless scatter. Additionally, while our AGC and SHC data were screened using the same metrics and therefore are directly comparable, the diversity of screening criteria applied to zircon studies could pose additional challenges when considering global comparisons or compilations of large datasets from across laboratories.

Data, Materials, and Software Availability. Zircon CL images data have been deposited in Zenodo (80). All study data are included in the article and/or supporting Information.

ACKNOWLEDGMENTS. We thank Noriko Kita, Peter Sobol, and Mike Spicuzza for assistance in the WiscSIMS lab, Bil Schneider for SEM assistance, and Drae Rogers for sample polishing. This work was supported by NSF EAR-2136782, awarded to T.B.B. and A.M.B., and by NSF DGE-1747503 awarded to E.E.M. WiscSIMS is supported by NSF EAR-2004618 and UW-Madison. This project has received funding from the European Research Council under the European Union's Horizon 2020 research and innovation program (Grant agreement No. 856555). Fieldwork and collection of the Saglek-Hebron samples was supported by NSERC Grants to J.O. (RGPIN 435589-2013) and H.R. (RGPIN-2015-03982 and RGPIN-477144-2015). Acasta Gneiss samples were provided from the legacy collection of Sam Bowring. We thank T. Harrison, the PNAS editorial staff, Elizabeth Bell, and one anonymous reviewer for constructive comments.

Author affiliations: [a]Department of Geoscience, University of Wisconsin-Madison, WI; [b]Department of Earth Sciences, Carleton University, Ottawa, ON, Canada; and [c]Department of Earth and Environmental Sciences, University of Ottawa, Ottawa, ON, Canada

1. S. A. Wilde, J. W. Valley, W. H. Peck, C. M. Graham, Evidence from detrital zircons for the existence of continental crust and oceans on the Earth 4.4 Gyr ago. *Nature* **409**, 175–178 (2001).
2. J. W. Valley, W. H. Peck, E. M. King, S. A. Wilde, A cool early Earth. *Geology* **30**, 351–354 (2002).
3. T. M. Harrison, Hadean Earth (Springer, 2020).
4. S. B. Shirey, S. H. Richardson, Start of the Wilson cycle at 3 Ga shown by diamonds from subcontinental mantle. *Science* **333**, 434–436 (2011).
5. J.-F. Moyen, H. Martin, Forty years of TTG research. *Lithos* **148**, 312–336 (2012).
6. N. Arndt, How did the continental crust form: No basalt, no water, no granite. *Precambrian Res.* **397**, 107196 (2023).
7. E. Belousova, W. L. Griffin, S. Y. O'Reilly, N. Fisher, Igneous zircon: Trace element composition as an indicator of source rock type. *Contrib. Mineral. Petrol.* **143**, 602–622 (2002).
8. C. Grimes, J. Wooden, M. Cheadle, B. John, "Fingerprinting" tectono-magmatic provenance using trace elements in igneous zircon. *Contrib. Mineral. Petrol.* **170**, 1–26 (2015).
9. T. L. Grove, C. B. Till, Melting the Earth's Upper Mantle in the Encyclopedia of Volcanoes (Elsevier, 2015), pp. 35–47.
10. B.-M. Jahn, A. Glikson, J. Peucat, A. Hickman, REE geochemistry and isotopic data of Archean silicic volcanics and granitoids from the Pilbara Block, Western Australia: Implications for the early crustal evolution. *Geochim. Cosmochim. Acta* **45**, 1633–1652 (1981).
11. N. Arndt, Archean Komatiites in Developments in Precambrian Geology (Elsevier, 1994), pp. 11–44.
12. H. Martin, J.-F. Moyen, R. Rapp, The sanukitoid series: Magmatism at the Archaean-Proterozoic transition. *Earth Environ. Sci. Trans. R. Soc. Edinb.* **100**, 15–33 (2009).
13. D. R. Mole *et al.*, Archean komatiite volcanism controlled by the evolution of early continents. *Proc. Natl. Acad. Sci. U.S.A.* **111**, 10083–10088 (2014).

14. C. Herzberg, K. Condie, J. Korenaga, Thermal history of the Earth and its petrological expression. *Earth Planet. Sci. Lett.* **292**, 79–88 (2010).
15. J. Ganne, X. Feng, Primary magmas and mantle temperatures through time. *Geochem. Geophys. Geosyst.* **18**, 872–888 (2017).
16. B. J. Foley, Timescale of short-term subduction episodicity in convection models with grain damage: Applications to Archean tectonics. *J. Geophys. Res. Solid Earth* **125**, e2020JB020478 (2020).
17. M. Guo, J. Korenaga, The combined Hf and Nd isotope evolution of the depleted mantle requires Hadean continental formation. *Sci. Adv.* **9**, eade2711 (2023).
18. W. B. Moore, A. A. G. Webb, Heat-pipe earth. *Nature* **501**, 501–505 (2013).
19. J. H. Bedard, L. B. Harris, P. C. Thurston, The hunting of the snArc. *Precambrian Res.* **229**, 20–48 (2013).
20. T. E. Johnson, M. Brown, B. J. Kaus, J. A. VanTongeren, Delamination and recycling of Archaean crust caused by gravitational instabilities. *Nat. Geosci.* **7**, 47–52 (2014).
21. M. J. Van Kranendonk *et al.*, Making it thick: A volcanic plateau origin of Palaeoarchean continental lithosphere of the Pilbara and Kaapvaal cratons. *Geol. Soc. Lond. Spec. Publ.* **389**, 83–111 (2015).
22. O. Nebel *et al.*, When crust comes of age: On the chemical evolution of Archaean, felsic continental crust by crustal drip tectonics. *Philos. Trans. R. Soc. A Math. Phys. Eng. Sci.* **376**, 20180103 (2018).
23. N. Drabon *et al.*, Heterogeneous Hadean crust with ambient mantle affinity recorded in detrital zircons of the Green Sandstone Bed, South Africa. *Proc. Natl. Acad. Sci. U.S.A.* **118**, e2004370118 (2021).
24. N. Drabon *et al.*, Destabilization of long-lived hadean Protocrust and the onset of pervasive hydrous melting at 3.8 Ga. *AGU Adv.* **3**, e2021AV000520 (2022).
25. N. Drabon, H. M. Kirkpatrick, G. R. Byerly, J. L. Wooden, Trace elements in zircon record changing magmatic processes and the multi-stage build-up of Archean proto-continental crust. *Geochim. Cosmochim. Acta* **373**, 136–150 (2024).
26. S. A. Bowring, I. S. Williams, Priscoan (4.00–4.03 Ga) orthogneisses from northwestern Canada. *Contrib. Mineral. Petrol.* **134**, 3–16 (1999).
27. J. R. Reimink, T. Chacko, R. A. Stern, L. M. Heaman, Earth's earliest evolved crust generated in an Iceland-like setting. *Nat. Geosci.* **7**, 529–533 (2014).
28. K. Collerson "Ion microprobe zircon geochronology of the Uivak gneisses: Implications for the evolution of early terrestrial crust in the North Atlantic Craton" in *Cross Section of Archean Crust*, (1983a).
29. K. D. Collerson, The Archean gneiss complex of northern Labrador. 2. Mineral ages, secondary isochrons, and diffusion of strontium during polymetamorphism of the Uivak gneisses. *Can. J. Earth Sci.* **20**, 707–718 (1983b).
30. T. Komiya *et al.*, A prolonged granitoid formation in Saglek Block, Labrador: Zonal growth and crustal reworking of continental crust in the Eoarchean. *Geosci. Front.* **8**, 355–385 (2017).
31. B. Wasilewski, J. O'Neil, H. Rizo, J.-L. Paquette, A.-M. Gannoun, Over one billion years of Archean crust evolution revealed by zircon U-Pb and Hf isotopes from the Saglek-Hebron complex. *Precambrian Res.* **359**, 106092 (2021).
32. J. R. Reimink, T. Chacko, R. A. Stern, L. M. Heaman, The birth of a cratonic nucleus: Lithogeochemical evolution of the 4.02–2.94 Ga Acasta Gneiss Complex. *Precambrian Res.* **281**, 453–472 (2016).
33. J. R. Reimink *et al.*, Petrogenesis and tectonics of the Acasta Gneiss Complex derived from integrated petrology and 142Nd and 182W extinct nuclide-geochemistry. *Earth Planet. Sci. Lett.* **494**, 12–22 (2018).
34. A. Bauer *et al.*, Hafnium isotopes in zircons document the gradual onset of mobile-lid tectonics. *Geochem. Perspect. Lett.* **14**, 1–6 (2020).
35. W. F. McDonough, S.-S. Sun, The composition of the Earth. *Chem. Geol.* **120**, 223–253 (1995).
36. E. E. Mixon *et al.*, Mechanisms for generating elevated zircon δ18O in Archean crust: Insights from the Saglek–Hebron complex, Canada. *Earth Planet. Sci. Lett.* **624**, 118443 (2023).
37. C. Spencer *et al.*, Disparities in oxygen isotopes of detrital and igneous zircon identify erosional bias in crustal rock record. *Earth Planet. Sci. Lett.* **577**, 117248 (2022).
38. P. W. Hoskin, Trace-element composition of hydrothermal zircon and the alteration of Hadean zircon from the Jack Hills, Australia. *Geochim. Cosmochim. Acta* **69**, 637–648 (2005).
39. A. J. Cavosie, J. W. Valley, S. A. Wilde *et al.*, Correlated microanalysis of zircon: Trace element, δ18O, and U-Th–Pb isotopic constraints on the igneous origin of complex >3900 Ma detrital grains. *Geochim. Cosmochim. Acta* **70**, 5601–5616 (2006).
40. E. A. Bell, P. Boehnke, T. M. Harrison, Recovering the primary geochemistry of Jack Hills zircons through quantitative estimates of chemical alteration. *Geochim. Cosmochim. Acta* **191**, 187–202 (2016).
41. A. M. Bauer, C. M. Fisher, J. D. Vervoort, S. A. Bowring, Coupled zircon Lu–Hf and U-Pb isotopic analyses of the oldest terrestrial crust, the> 4.03 Ga Acasta Gneiss Complex. *Earth Planet. Sci. Lett.* **458**, 37–48 (2017).
42. A. M. Bauer, J. D. Vervoort, C. Fisher, Unraveling the complexity of zircons from the 4.0–2.9 Ga Acasta Gneiss Complex. *Geoch. Cosm. Act.* **283**, 85-102 (2020).
43. D. Rubatto, J. Hermann, Experimental zircon/melt and zircon/garnet trace element partitioning and implications for the geochronology of crustal rocks. *Chem. Geol.* **241**, 38–61 (2007).
44. L. L. Claiborne *et al.*, "Zircon as magma monitor: Robust, temperature-dependent partition coefficients from glass and zircon surface and rim measurements from natural systems" in *Microstructural Geochronology: Planetary Records Down to Atom Scale*, D. E. Moser, F. Corfu, J. R. Darling, S. M. Reddy, K. Tait, Eds. (American Geophysical Union, 2018), chap. 1, pp. 1–33.
45. A. D. Burnham, Key concepts in interpreting the concentrations of the rare earth elements in zircon. *Chem. Geol.* **551**, 119765 (2020).
46. S. M. Aarons *et al.*, Titanium isotopes constrain a magmatic transition at the Hadean-Archean boundary in the Acasta Gneiss complex. *Sci. Adv.* **6**, eabc9959 (2020).
47. Q. Zhang *et al.*, No evidence of supracrustal recycling in Si–O isotopes of Earth's oldest rocks 4 Ga ago. *Sci. Adv.* **9**, eadf0693 (2023).
48. J. R. Reimink, J. H. Davies, A. M. Bauer, T. Chacko, A comparison between zircons from the Acasta Gneiss complex and the Jack Hills region. *Earth Planet. Sci. Lett.* **531**, 115975 (2020).
49. T. Carley *et al.*, Zircon–modeled melts shed light on the formation of Earth's crust from the Hadean to the Archean. *Geology* **50**, 1028–1032 (2022).
50. B. Wasilewski, J. O'Neil, H. Rizo, Archean crustal evolution of the Saglek-Hebron complex, Northern Labrador, revealed from coupled 147–146Sm–143- 142Nd systematics. *Earth Planet. Sci. Lett.* **594**, 117735 (2022).
51. J. Valley *et al.*, 4.4 billion years of crustal maturation: Oxygen isotope ratios of magmatic zircon. *Contrib. Mineral. Petrol.* **150**, 561–580 (2005).
52. C. E. Bucholz, C. J. Spencer, Strongly peraluminous granites across the archean–proterozoic transition. *J. Petrol.* **60**, 1299–1348 (2019).
53. A. Kemp *et al.*, Magmatic and crustal differentiation history of granitic rocks from Hf–O isotopes in zircon. *Science* **315**, 980–983 (2007).
54. B. Dhuime, C. J. Hawkesworth, P. A. Cawood, C. D. Storey, A change in the geodynamics of continental growth 3 billion years ago. *Science* **335**, 1334–1336 (2012).
55. T. Naeraa *et al.*, Hafnium isotope evidence for a transition in the dynamics of continental growth 3.2 Gyr ago. *Nature* **485**, 627–630 (2012).
56. A. Rozel, G. J. Golabek, C. Jain, P. J. Tackley, T. Gerya, Continental crust formation on early Earth controlled by intrusive magmatism. *Nature* **545**, 332–335 (2017).
57. N. M. Roberts, J. D. Hernández-Montenegro, R. M. Palin, Garnet stability during crustal melting: Implications for chemical mohometry and secular change in arc magmatism and continent formation. *Chem. Geol.* **659**, 122142 (2024).
58. A. Pourteau *et al.*, TTG generation by fluid-fluxed crustal melting: Direct evidence from the Proterozoic Georgetown Inlier, NE Australia. *Earth Planet. Sci. Lett.* **550**, 116548 (2020).
59. L. Profeta *et al.*, Quantifying crustal thickness over time in magmatic arcs. *Sci. Rep.* **5**, 17786 (2015).
60. M. Tang, W.-Q. Ji, X. Chu, A. Wu, C. Chen, Reconstructing crustal thickness evolution from europium anomalies in detrital zircons. *Geology* **49**, 76–80 (2021).
61. A. Roman, N. Arndt, Differentiated Archean oceanic crust: Its thermal structure, mechanical stability and a test of the sagduction hypothesis. *Geochim. Cosmochim. Acta* **278**, 65–77 (2020).
62. J. van Hunen, A. P. van den Berg, Plate tectonics on the early Earth: Limitations imposed by strength and buoyancy of subducted lithosphere. *Lithos* **103**, 217–235 (2008).
63. B. Wasilewski, J. O'Neil, H. Rizo, Geochemistry and petrogenesis of the early Archean mafic crust from the Saglek-Hebron Complex (Northern Labrador). *Precambrian Res.* **328**, 321–343 (2019).
64. J.-F. Moyen, J. Van Hunen, Short-term episodicity of Archaean plate tectonics. *Geology* **40**, 451–454 (2012).
65. B. Fu *et al.*, Ti-in-zircon thermometry: Applications and limitations. *Contrib. Mineral. Petrol.* **156**, 197–215 (2008).
66. M. D. Hopkins, T. M. Harrison, C. E. Manning, Constraints on Hadean geodynamics from mineral inclusions in >4 Ga zircons. *Earth Planet. Sci. Lett.* **298**, 367–376 (2010).
67. J. W. Valley *et al.*, Hadean age for a post-magma-ocean zircon confirmed by atom-probe tomography. *Nat. Geosci.* **7**, 219–223 (2014).
68. T. Iizuka *et al.*, Reworking of Hadean crust in the Acasta gneisses, northwestern Canada: Evidence from in-situ Lu–Hf isotope analysis of zircon. *Chem. Geol.* **259**, 230–239 (2009).
69. S. J. Mojzsis *et al.*, Component geochronology in the polyphase ca. 3920 Ma Acasta Gneiss. *Geochim. Cosmochim. Acta* **133**, 68–96 (2014).
70. N. Rayner, R. Stern, S. Carr, Grain-scale variations in trace element composition of fluid-altered zircon, Acasta Gneiss Complex, northwestern Canada. *Contrib. Mineral. Petrol.* **148**, 721–734 (2005).
71. L. Schiøtte, W. Compston, D. Bridgwater, Ion probe U–Th–Pb zircon dating of polymetamorphic orthogneisses from northern Labrador, Canada. *Can. J. Earth Sci.* **26**, 1533–1556 (1989).
72. M. A. Kusiak *et al.*, Peak to post-peak thermal history of the Saglek Block of Labrador: A multiphase and multi-instrumental approach to geochronology. *Chem. Geol.* **484**, 210–223 (2018).
73. A. Salacińska *et al.*, Complexity of the early Archean Uivak Gneiss: Insights from Tigigakyuk Inlet, Saglek Block, Labrador, Canada and possible correlations with South West Greenland. *Precambrian Res.* **315**, 103–119 (2018).
74. T. B. Blum, K. Kitajima, N. Kita, J. W. Valley, "Analysis of trace elements in zircon at high mass resolving power using forward-geometry secondary ion mass spectrometry" in *Goldschmidt 2023 Conference* (GOLDSCHMIDT, 2023).
75. E. M. Cameron *et al.*, Evidence for oceans pre-4300 Ma confirmed by preserved igneous compositions in Hadean zircon. *Am. Mineral.* **109**, 1–10 (2024).
76. F. Corfu, J. M. Hanchar, P. W. Hoskin, P. Kinny, Atlas of zircon textures. *Rev. Mineral. Geochem.* **53**, 469–500 (2003).
77. X.-L. Wang *et al.*, Influence of radiation damage on Late Jurassic zircon from southern China: Evidence from in situ measurements of oxygen isotopes, laser Raman, U-Pb ages, and trace elements. *Chem. Geol.* **389**, 122–136 (2014).
78. R. Pidgeon, A. Nemchin, M. Roberts, M. J. Whitehouse, J. Bellucci, The accumulation of non-formula elements in zircons during weathering: Ancient zircons from the Jack Hills, Western Australia. *Chem. Geol.* **530**, 119310 (2019).
79. J. Liebmann, C. J. Spencer, C. L. Kirkland, X.-P. Xia, J. Bourdet, Effect of water on δ18O in zircon. *Chem. Geol.* **574**, 120243. (2021).
80. E. E. Mixon *et al.*, AGC-SHC-Zircon CL images. Zenodo. https://zenodo.org/doi/10.5281/zenodo.12573106. Deposited 27 June 2024.